Missile Guidance Design Tradeoffs for High-Altitude Air Defense

F. William Nesline* and Paul Zarchan†
Raytheon Company, Bedford, Massachusetts

Practical design considerations for a high-altitude radar-guided air defense missile are presented. Three major contributors to miss distance are discussed—the radar signal return, the radar tracking seeker component imperfections, and the missile response limitations. At high altitude, glint may be the major contaminant in the radar signal. In addition, seeker component imperfections such as imperfect gimbal stabilization, radome refraction slope, and seeker gyro acceleration sensitivity cause stability and miss distance problems that the guidance system designer must solve. Finally, the missile response to guidance commands is limited by reduced acceleration capability, increased response time, and control fin rate saturation. The miss distance sensitivity of each of these factors is discussed and, in addition, the stability issues associated with the unwanted feedback paths created by component imperfections are addressed. Numerical examples are presented showing the significance of including practical hardware imperfections in preliminary design if performance goals at high altitude are to be met when the system is built. The paper provides a perspective of real-world problems which in theoretical investigations are often viewed as secondary issues, but which in fact may be the dominant factors that dictate the guidance and control system design parameters.

Introduction

SUCCESSFUL missile guidance for high-altitude air defense poses special problems for the radar sensor as well as for the missile flight control system. Targets at high altitude can be large so that the radar return contains significant glint. Glint is a noise that is induced onto the angular direction of the target by small rotations in the relative target/missile geometry.[1-3] Since high-altitude targets can be large airplanes that do not rotate very much, the glint is large and of low bandwidth. The low bandwidth decreases the effectiveness of normal filtering. In addition to glint, the radar signal contains receiver noise and fading noise. Receiver noise is a range-dependent noise whose rms value reduces with decreasing range and whose bandwidth is wide compared to the guidance bandwidth. Fading noise is a range-independent noise.[3]

The radar signal passes through the radome to the seeker antenna and then to the radar receiver. The seeker antenna is gimballed with respect to the missile to allow target acquisition and tracking.[4] The gimbal system is stabilized in space using a rate gyro as a sensor. The degree to which the gimbal is stabilized determines the accuracy of the target line-of-sight rate measurement. Important factors in stabilization are the seeker stabilization loop gain and the drift rate and acceleration sensitivity of the seeker gyro. Each component imperfection in the seeker may be represented as an input signal or as a gain in the dynamic block diagram that represents missile performance. The miss distance sensitivity is then obtained using that block diagram in forward Monte Carlo simulations or in adjoint miss distance simulations.[5,6]

At high altitudes, the low dynamic pressure of the air limits the acceleration capability of both the target and the missile, limits the missile response time that is achievable, and causes large control fin deflections which in turn may lead to rate saturation of the control actuator in response to the acceleration commands from guidance.[7] Each of these factors is a source of miss distance that is examined by nonlinear forward simulations and by linearized adjoint solutions of the simulations.

Received Aug. 23, 1982; revision received Jan. 17, 1983.

*Chief Systems Engineer, System Design Laboratory, Missile Systems Division. Associate Fellow AIAA.

†Principal Engineer, System Design Laboratory, Missile Systems Division. Member AIAA.

Idealized Miss Distance Calculations

The planar dynamics of the radar homing system shown in Fig. 1 indicates the dynamics of the various parts of the missile guidance system.[8,9] The seeker contains a tracking loop and a simplified stabilization loop. In addition, parameters that represent unwanted, or parasitic, feedback paths for radome refraction slope and for gyro acceleration sensitivity are shown. The idealized system, often discussed in the literature, has zero radome refraction slope, zero gyro acceleration sensitivity, and infinite stabilization loop gain. The noise filter attenuates the radar boresight error noise to develop a smoothed estimate of the line-of-sight rate. The guidance law converts the line-of-sight rate estimate into acceleration commands for the flight control system. For the idealized system, the guidance transfer function from line-of-sight rate to missile acceleration ($n_L/\dot{\lambda}$) is

$$\left.\frac{n_L}{\dot{\lambda}}\right|_{\text{idealized}} = \frac{N' V_c (1 - S^2/\omega_z^2)}{(1+ST_I)(1+ST_N)(1+ST_a)[1+(2\zeta_a/\omega_a)S+(S^2/\omega_a^2)]} \tag{1}$$

where N' is the effective navigation ratio, V_c the closing velocity, and T_I and T_N the seeker and noise filter time constants. The numerator has two zeros, a minimum phase and a nonminimum phase. The nonminimum phase zero ω_z is determined by the aerodynamic configuration and is typical of tail-controlled missiles. The flight control system (autopilot) time constant T_a, damping ζ_a, and natural frequency ω_a are typical parameters in an operational three-loop autopilot.[7] The transfer function of Eq. (1) is always stable because the unwanted (parasitic) feedback paths of Fig. 1 have been neglected and because perfect stabilization has been assumed. Therefore,

$$\epsilon/\dot{\theta}\,|_{\text{idealized}} = 0 \tag{2}$$

$$\epsilon/n_L\,|_{\text{idealized}} = 0 \tag{3}$$

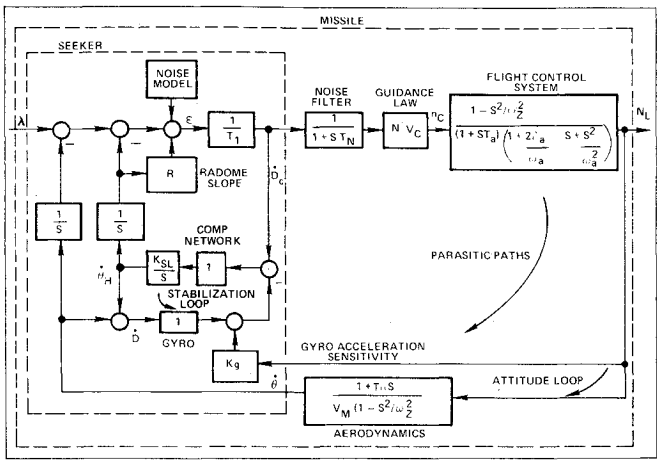

Fig. 1 Missile system dynamics.

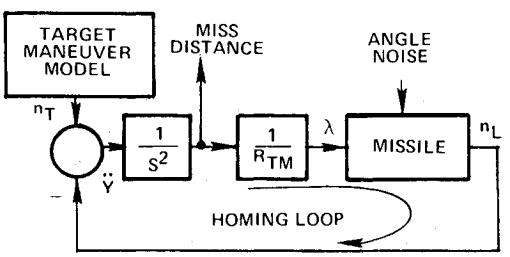

Fig. 2 Miss distance dynamics.

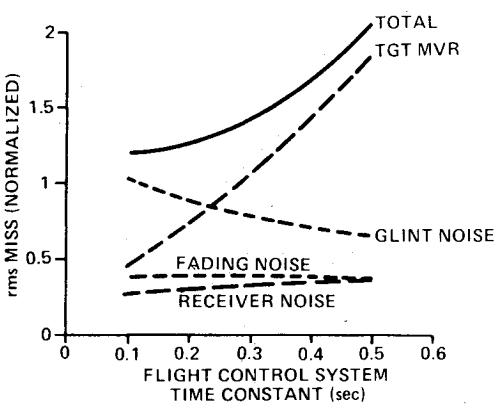

Fig. 3 Miss distance decreases with decreasing flight control system time constant for ideal system.

For a nominal ideal system, the tracking time constant is set by seeker tracking dynamics, the noise filter time constant is set by radar signal and noise spectral content, the effective navigation ratio is set by knowledge of the properties of proportional navigation, the closing velocity is measured by the radar using Doppler or range rate information, the flight control zeroes are determined by the missile aerodynamics, and the three flight control poles are determined by the missile and the flight control system, i.e., the aerodynamics, structural dynamics, actuators, instruments, and autopilot gains. The frequency of the quadratic autopilot pole pair is determined by the aerodynamic moment slope with respect to angle of attack M_α, and the damping of the quadratic pair is set by stability considerations. Therefore, the autopilot real pole $(-1/T_a)$ is the primary adjustable parameter for the ideal guidance system.

The miss distance of this ideal linear system, using the trajectory dynamic model of Fig. 2, was calculated for the following nominal set of parameters for various values of autopilot time constant T_a:

T_α = 2 s (aerodynamic turning rate time constant)

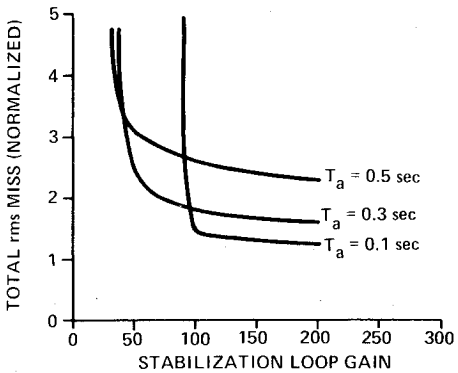

Fig. 4 Stabilization loop gain requirements become more stringent with decreasing flight control system time constant.

T_I = 0.1 s (seeker tracking time constant)
T_N = 0.15 s (noise filter time constant)
N' = 3 (effective navigation ratio)
V_c = 4500 ft/s (closing velocity)
V_M = 2500 ft/s (missile velocity)
ω_z = 30 rad/s (flight control system zeroes)
ω_a = 20 rad/s (flight control system natural frequency)
ζ_a = 0.7 (flight control system damping)
K_{SL} = 100 rad/s (stabilization loop gain)

The results, plotted in Fig. 3, show the effect of each of the components of miss as well as the total miss. For a non-maneuvering target, the major source of miss is glint and the larger the time constant, the smaller the glint miss. On the other hand, a target maneuver will result in increased miss as time constant increases. For the case considered, the total miss is flat out to 0.1 s and increases for larger values of time constant. The optimal choice of time constant depends upon the relative magnitudes of target maneuver and glint chosen for the design. For the inputs chosen, the flight control system time constant that minimized the miss distance is 0.1 s. We shall see below that when realistic constraints are considered, larger values of time constant may be required.

Seeker Component Imperfections

The seeker component imperfections considered are the stabilization loop gain and bandwidth, the radome refraction slope, and the seeker gyro acceleration sensitivity.

Seeker Stabilization

The seeker has a gyro-controlled stabilization loop to prevent missile pitching motion from contaminating the line-of-sight rate to the target. Figure 1 shows a simple first-order stabilization loop consisting of a gain and an integrator. The degree of stabilization achieved depends upon the gain K_{SL}. For such a simple stabilization loop, K_{SL} is also the stabilization bandwidth. For $R=0$, $K_g=0$, and the parameters as listed previously, the miss distance variation with stabilization loop gain K_{SL} is shown in Fig. 4. The miss distance for any finite gain is always larger than that of the ideal, infinite gain system, but relatively large stabilization loop gains approach the perfect stabilization loop performance. However, it is important to note that as the stabilization loop gain is reduced, a point is reached at which the miss distance increases very rapidly. A stability analysis of the missile guidance system shows that it is unstable for values of stabilization loop gain below that value.

Imperfect stabilization couples body motion into the forward path resulting in the transfer function

$$\left.\frac{\epsilon}{\dot\theta}\right|_{\substack{\text{imperfect}\\ \text{stabilization}}} = \frac{-T_I S}{K_{SL}(1+ST_I+S^2T_I/K_{SL})} \approx \frac{-T_I S}{K_{SL}(1+ST_I)(1+S/K_{SL})} \quad (4)$$

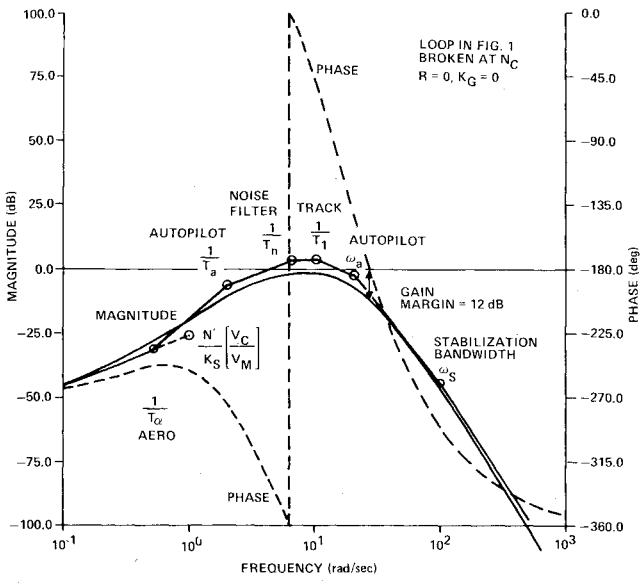

Fig. 5 Bode plot shows that increasing stabilization loop gain improves stability margins of attitude loop.

The attitude path open-loop transfer function becomes

$$HG\Big|_{\substack{\text{imperfect}\\ \text{stabilization}}} \approx \frac{N' V_c S(1+ST_\alpha)}{K_{SL} V_M (1+ST_1)(1+S/K_{SL})} * \frac{1}{(1+ST_N)(1+ST_a)[1+(2\zeta_a/\omega_a)S+(S^2/\omega_a^2)]} \tag{5}$$

Figure 5 shows a frequency response of an attitude loop with the corner frequencies of all the components marked. For the parameters used, the gain margin is 12 dB. This gain margin degrades as the autopilot time constant (or any of the other time constants) is reduced. In addition, the gain constant of this attitude loop is $(N' V_c/K_{SL} V_M)$. Therefore the gain margin improves as the stabilization loop gain increases. The value of the stabilization gain at the stability limit shown in Fig. 6 correlates well with the value that generates the large miss distance in Fig. 4. Of course, a practical value for the stabilization loop gain should yield at least a 6 dB gain margin, or perhaps more if the aerodynamics are not well known. A practical upper limit on the stabilization loop gain might be 100 or so. In this case, the curves in Fig. 6 show that the fastest autopilot time constant achievable is 0.24 s. If a faster autopilot is wanted, adjustment of the tracking time constant or noise filter time constant is required. Since practical considerations dictate an upper limit on the stabilization bandwidth, the autopilot time constant chosen must be large enough to guarantee stability.

Another method of achieving high-stabilization loop gain in a reasonable stabilization loop bandwidth is to frequency shape the stabilization loop with a lag-lead network. If the network is of the form

$$\text{NTWK} = \frac{W_2}{W_1}\frac{(1+S/W_2)}{(1+S/W_1)} \tag{6}$$

the stabilization loop crossover frequency will remain unchanged. However, the network will effectively reduce the gain of the attitude loop at the lower frequencies, thus making the stabilization loop gain appear larger. The larger the frequency difference between the lead and lag, the larger will be the apparent gain reduction in the attitude loop. Increasing the lead frequency will increase the frequency to which the attitude loop gain reduction will last.

To illustrate the benefit of frequency shaping, the stabilization loop gain was chosen to result in a slightly unstable attitude path whose open-loop transfer function was

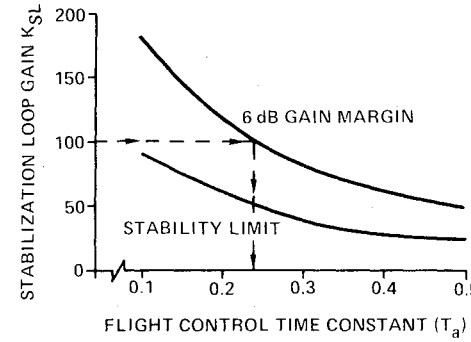

Fig. 6 Stabilization loop gain requirements relax with increasing flight control system time constant.

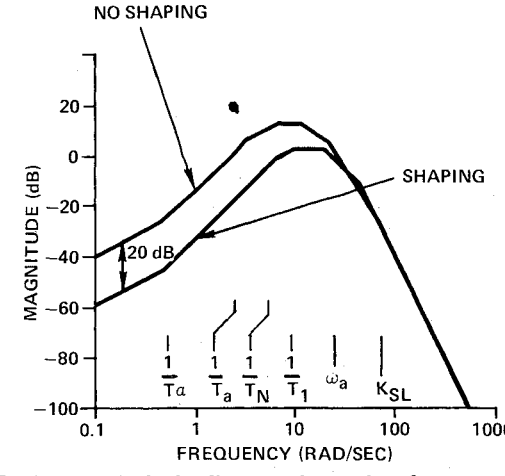

Fig. 7 Asymptotic bode diagram shows that frequency shaping reduces attitude loop gain at lower frequencies.

$$HG\Big|_{\text{no shaping}} = \frac{0.108S(1+S/0.5)}{(1+S/3.33)(1+S/6.67)(1+S/10)} * \frac{1}{(1+[2(0.7)/20]S+S^2/20^2)(1+S/50)} \tag{7}$$

Inserting the following network into the stabilization loop

$$\text{NTWK} = \frac{10(1+S/30)}{(1+S/3)} \tag{8}$$

stabilizes the attitude loop with 100 deg of phase margin and 6.9 dB of gain margin. The new attitude path open-loop transfer function is

$$HG\Big|_{\substack{\text{freq}\\ \text{shaping}}} = \frac{0.0108S(1+S/0.5)(1+S/3)}{(1+S/3.33)(1+S/6.67)(1+S/9.5)} * 1/(1+2(0.7)S/20+S^2/20^2)(1+2(0.55)S/40+S^2/40^2) \tag{9}$$

For this case the attitude loop gain was reduced by 20 dB, as can be seen from the asymptotic Bode diagram of Fig. 7.

Radome Refraction Slope

At high altitudes, missile guidance commands cause large pitching or yawing motions that change the direction of the radar wave through the radome. This change, coupled with a different value for radome refraction, produces an apparent target motion similar to true target motion.[8-11] In Fig. 1, the radome refraction slope is shown as a constant multiplier on the angle of the seeker with respect to the missile centerline. The effect of any given radome slope on miss distance

depends upon the aerodynamic turning rate time constant T_α. For the relatively small values of T_α found at low altitudes,[12] radome slope is not of much significance, as seen in Fig. 8. However, T_α increases with altitude and at altitudes where T_α is large, the allowable radome slope range reduces sharply as shown in Table 1, taken from Fig. 8.

Stability problems are created by the radome because it couples body motion into the forward path, resulting in

$$\left.\frac{\epsilon}{\dot{\theta}}\right|_{\text{radome}} \approx -\frac{T_I R(1+S/RK_{SL})}{(1+ST_I)(1+S/K_{SL})} \tag{10}$$

The attitude path open loop transfer function becomes

$$\left.HG\right|_{\text{radome}} \approx \frac{N'V_c R}{V_M}\frac{(1+T_\alpha S)(1+S/RK_{SL})}{(1+ST_I)(1+S/K_{SL})(1+ST_N)} * \frac{1}{(1+ST_a)[1+(2\zeta_a/\omega_a)S+S^2/\omega_a^2]} \tag{11}$$

If the attitude closed-loop transfer function is written, the coefficient of the first-order term in the denominator is $T+N'(V_c/V_M)RT_\alpha$ where T is a composite constant.

Clearly, the significant effect is not R alone, but the product $N'RT_\alpha(V_c/V_M)$. Therefore, the stability (and the miss distance) depends upon the radome, the missile aerodynamics, and the engagement parameters, e.g., closing velocity and missile velocity.

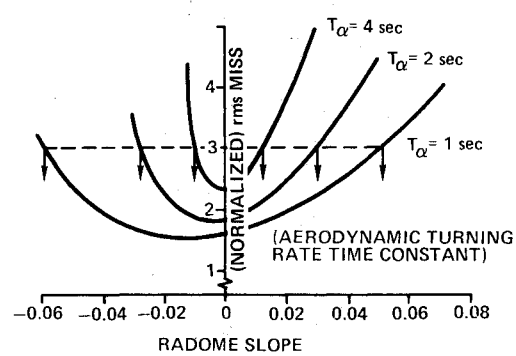

Fig. 8 Increasing turning rate time constant makes miss more sensitive to radome slope.

Table 1 Radome slopes for maximum miss = 3

T_α	Range of allowable radome slopes
1	−0.059, 0.052
2	−0.028, 0.03
4	−0.01, 0.013

In addition to affecting miss distance, radome slope creates characteristic stability problems. The root locus was calculated and is plotted in Fig. 9, which shows how the roots migrate as the radome refraction slope R changes from its nominal value of zero. As the radome slope goes negative, the low-frequency pole pair loses its damping and crosses the imaginary axis at about 1.6 rad/s. This low-frequency oscillation increases the miss distance. As the radome slope R goes positive, the high-frequency pole pair loses its damping and crosses the imaginary axis at about 25 rad/s. This high-frequency instability generally occurs at a large value of radome slope compared to the capability of modern radomes.

To further illustrate stability considerations, missile acceleration time histories for negative, zero, and positive radome slopes due to a 2 g target maneuver are shown in Fig. 10. The nominal values were used, along with $T_a = 0.3$ s, $T_\alpha = 4$ s, and $K_{SL} = 100$. The root locus predicted the negative slope to yield an instability at 0.25 Hz and a positive slope to yield an instability at 3.9 Hz. These values are confirmed in Fig. 10.

System radome sensitivity also depends on the autopilot time constant T_a. As can be seen from Fig. 11, decreasing the autopilot time constant makes system performance more sensitive to radome slope. Therefore, radome specifications become tighter when smaller autopilot time constants are sought.

Gyro Acceleration Sensitivity

The gyro acceleration sensitivity, g-sensitive drift, creates a direct feedback path from the achieved acceleration to the measured antenna rate in space. This path becomes important at high closing velocity, a condition which occurs in short-range or high-altitude flights.

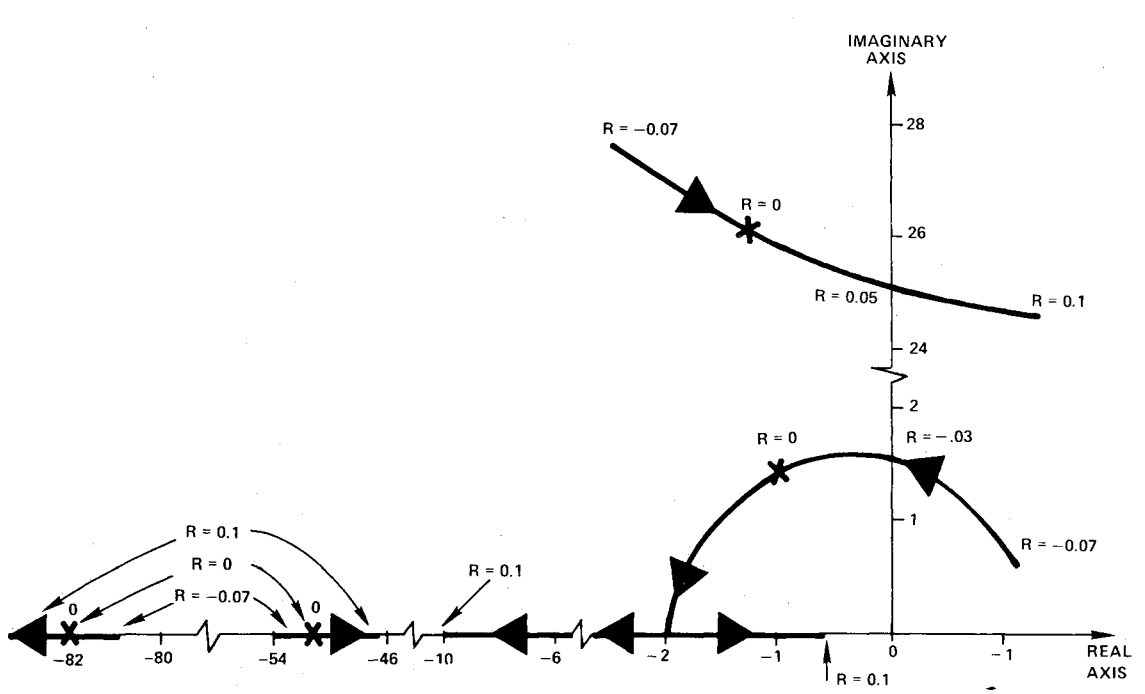

Fig. 9 Radome refraction slope root locus shows attitude loop can become unstable due to either positive or negative slopes.

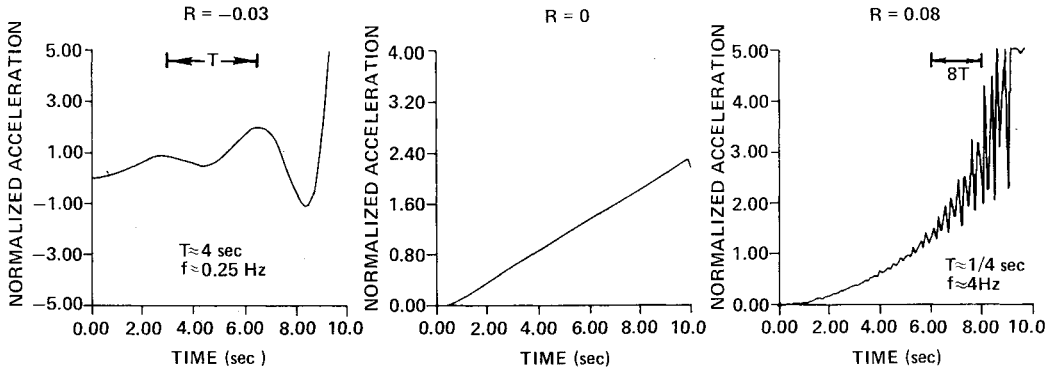

Fig. 10 Negative radome slopes can cause low-frequency oscillation and positive slopes can cause high-frequency oscillation.

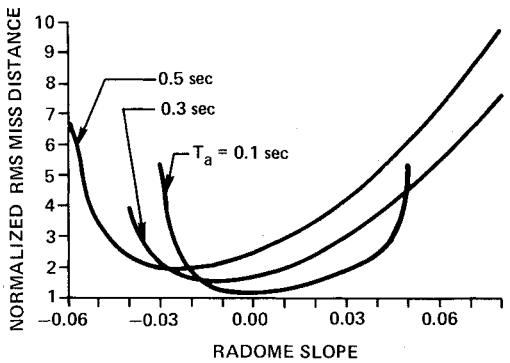

Fig. 11 Performance sensitivity to radome increases with decreasing autopilot time constant.

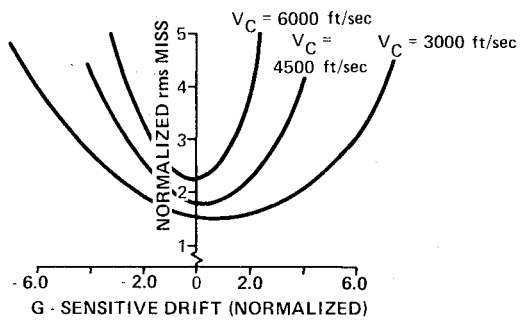

Fig. 12 Increasing closing velocity makes miss distance more sensitive to gyro acceleration sensitivity.

The parasitic transfer function (neglecting stabilization effects) becomes

$$\frac{\epsilon}{n_L}\bigg|_{g_{\text{sensitive}}} = \frac{T_1 K_g}{(1+ST_1)} \tag{12}$$

and the attitude path open-loop transfer function becomes

$$HG\big|_{g_{\text{sensitive}}} = \frac{-N' V_c K_g (1-S^2/\omega_z^2)}{(1+ST_1)(1+ST_N)(1+ST_a)} * \frac{1}{[1+(2\zeta_a/\omega_a)S+S^2/\omega_a^2]} \tag{13}$$

Closing velocity is important for this parasitic effect, since it directly multiplies the gyro acceleration sensitivity.

Typical miss distance vs gyro acceleration sensitivity curves is shown in Fig. 12, which shows that the miss distance degrades as the g-sensitive drift increases and that it increases dramatically as the closing velocity increases. For a given distance, high-closing-velocity engagements place significantly more stringent requirements on the g sensitivity.

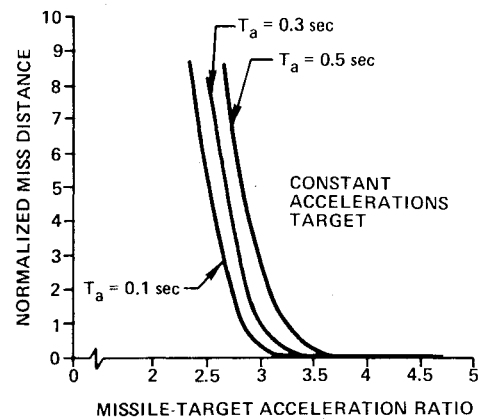

Fig. 13 Acceleration saturation influences system performance.

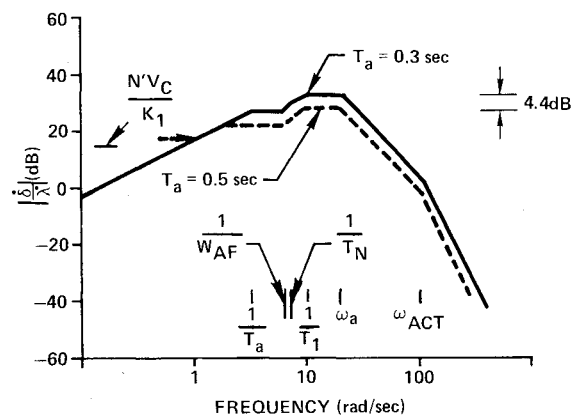

Fig. 14 Closed-loop asymptotic frequency response shows fin rate increases with decreasing autopilot time constant.

Unlike radome effects, the influence of gyro acceleration sensitivity on system performance is independent of the autopilot turning rate T_α time constant. The designer must select the rate gyro whose g sensitivity will allow the system to work at the high-closing-velocity end of the flight envelope.

Missile System Contributors to Miss

In addition to noise on the radar signal and imperfections in the seeker, the response limitations of the missile contribute to the miss distance and stability problems that the designer must solve. These limitations are both linear and nonlinear. The most significant linear effect is the missile response time, which has already been discussed in terms of T_a; and the most significant nonlinear effects discussed here are acceleration saturation and fin rate saturation. Other effects such as backlash and hysteresis may be important in particular cases, but they are not discussed in detail in this paper. The fun-

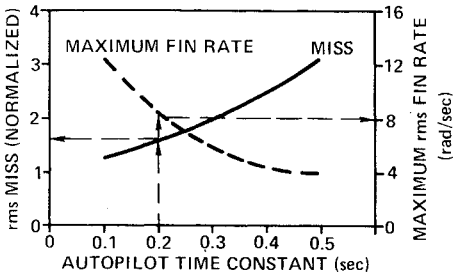

Fig. 15 Decreasing flight control system time constant improves performance at the expense of increased actuator requirements.

damental cause of acceleration saturation at high altitude is low dynamic pressure ($q=\frac{1}{2}\rho V^2$), and the fundamental cause of fin rate saturation is the response properties of the control fin actuator.

Limited Acceleration Capability

With the nominal system parameters, miss distance results were generated for a constant target maneuver disturbance, with the missile acceleration limit and autopilot time constant acting as parameters. Figure 13 shows that miss distance increases with decreasing missile/target acceleration advantage and increasing autopilot time constant. These effects are discussed many places in the literature (Ref. 12, for example). Therefore, the designer must insure that the airframe capability is sufficient to deal with the threat.

Limited Actuator Capability

At high altitude, the control fins must move at high rates to achieve rapidly the large control fin angles necessary to trim the missile. If the control fin actuator cannot attain these rates, instability can result.

The airframe and actuator transfer functions can be expressed as

$$\frac{n_L}{\delta}=\frac{K_1(1-S^2/\omega_z^2)}{1+(2\zeta_{AF}/\omega_{AF})S+(S^2/\omega_{AF}{}^2)}\ \text{(Airframe)} \tag{14}$$

$$\frac{\delta}{\delta_c}=\frac{1}{1+(2\zeta_{ACT}/\omega_{ACT})S+(S^2/\omega_{ACT}{}^2)}\ \text{(Actuator)} \tag{15}$$

The fin rate response, neglecting parasitic effects, due to line-of-sight rate becomes

$$\frac{\dot{\delta}}{\dot{\lambda}}_{\text{Idealized}}=\frac{N'V_c}{K_1}\frac{S[1+(2\zeta_{AF}/\omega_{AF})S+(S^2/\omega_{AF}{}^2]}{(1+ST_1)(1+ST_N)(1+ST_a)}\ *$$

$$1\Big/\left(1+\frac{2\zeta_a}{\omega_a}S+\frac{S^2}{\omega_a^2}\right)\left(1+\frac{2\zeta_{ACT}}{\omega_{ACT}}S+\frac{S^2}{\omega_{ACT}{}^2}\right) \tag{16}$$

With the nominal values and $\omega_{AF}=6$ rad/s, $\zeta_{AF}=0.05$, $\omega_{ACT}=100$, and $\zeta_{ACT}=0.5$, the closed-loop response can be calculated. Figure 14 presents the asymptotic gain approximations for two different autopilot time constants. The faster system ($T_a=0.3$ s) has more noise transmission and hence fin rate response than the slower ($T_a=0.5$ s). The slower system results in a 4.4 dB drop in fin rate response. Figure 15 quantifies these results in terms of rms miss distance and rms fin rate response as a function of the autopilot time constant. This figure shows an increase in the maximum fin rate as the autopilot time constant decreases. For the parameters used, this reduced autopilot time constant also results in reduced miss. The arrows in Fig. 15 show that a time constant of 0.2 s gives a miss of 1.7 and requires a fin rate of 8 rad/s. The designer must insure that the actuator supports the resultant fin rates required by the autopilot time constant in order to avoid instability at high altitude. If it does not, the autopilot time constant must be increased.

Therefore, the first step in design is to build an actuator that has a high enough rate limit to support the miss distance requirements. The second step is to introduce nonlinearities into the autopilot that will insure missile stability even if the actuator saturates.

Conclusions

At high altitude, system performance is dependent upon the radar return, seeker component imperfections, and missile response limitations. The seeker imperfections, such as imperfect gimbal stabilization, radome refraction slope, and rate gyro acceleration sensitivity, add unwanted feedback paths within the missile homing loop. These parasitic paths can cause miss distance and stability problems that the guidance system designer must recognize and solve. Finally, the missile response is limited by the aerodynamics and by the actuator system nonlinearities.

The examples presented in this paper indicate that all of the above factors must be considered for a successful and economical design. Minimization of the miss distance by time constant reduction must take into account the parasitic and nonlinear constraints. Failure to include the realistic constraints may cause the resultant design, when tested, either to be unstable or to result in larger miss distances than originally anticipated.

References

[1] Delano, R.H., "A Theory of Target Glint or Angle Scintillation in Radar Tracking," *Proceedings of IRE,* Vol. 41, Dec. 1953, pp. 1778-1784.

[2] Barton, D.K., *Radar Systems Analysis,* Prentice Hall, Inc., Englewood Cliffs, N.J., 1964, pp. 289-290.

[3] Skolnik, M., *Radar Handbook,* McGraw-Hill Book Co., New York, 1970, Chap. 28.

[4] Garnell, P. and East, D.J., *Guided Weapon Control Systems,* Pergamon Press, Oxford, England, 1977, pp. 168-178.

[5] Zarchan, P., "Complete Statistical Analysis of Nonlinear Missile Guidance Systems—SLAM," *Journal of Guidance and Control,* Vol. 2, Jan.-Feb. 1979, pp. 71-78.

[6] Laning, J.H. and Battin, T.H., *Random Processes in Automatic Control,* McGraw-Hill Book Co., New York, 1956.

[7] Nesline, F.W. and Zarchan, P., "A New Look at Classical vs Modern Homing Missile Guidance," *Journal of Guidance and Control,* Vol. 4, Jan.-Feb. 1981, pp. 78-85.

[8] Yost, D.J., Weckesser, L.B., and Mallalieu, R.C., "Technology Survey of Radomes for Anti-Air Homing Missiles," Johns Hopkins Applied Physics Lab., Rept. FS-80-022, March 1980.

[9] Keuhne, B.E., "An Assessment of Radome and Aero/Control Models for Simulating Boresight Errors in Homing Missiles," *Proceedings of AIAA Guidance and Control Conference,* Danvers, Mass., Aug. 1980, pp. 220-229.

[10] Phillips, T.L., "Anti-Aircraft Missile Guidance," *Electronic Progress,* Raytheon Co., March-April 1958, pp. 1-5.

[11] Travers, P., "Interceptor Dynamics," Unpublished lecture notes, Raytheon Co., circa 1971.

[12] Nesline, F.W., "Missile Guidance for Low Altitude Air Defense," *Journal of Guidance and Control,* Vol. 2, July-Aug. 1979, pp. 283-289.